RSC Advances

ROYAL SOCIETY OF CHEMISTRY

www.rsc.org/advances

RSC Advances

PAPER

Modeling EPR parameters of nitrogen containing conjugated radical cations

Received 00th January 20xx,
Accepted 00th January 20xx

DOI: 10.1039/x0xx00000x

www.rsc.org/

L. Hermosilla,* P. Calle and J. M. García de la Vega

The accuracy of DFT methodology on modeling isotropic hyperfine coupling constants (hfccs or a_{iso}) of conjugated radical cations containing ^{14}N nucleus, intermediates involved in many biological and chemical processes, is investigated. A set of 222 hfccs, belonging to 50 radical species, are computed at the following levels of theory: PBE0/N07D, B3LYP/6-31G, B3LYP/N07D, B3LYP/TZVP, and B3LYP/EPR-III, and compared to the available experimental values. In general, these five combinations of methods and basis sets estimate $a_{iso}(^1H)$ in good agreement with experimental data. Conversely, selection of the basis set is of fundamental importance for accurate prediction of the ^{14}N hfccs. A thorough analysis of the computed data allows us to establish that the best functional/basis set combination for obtaining accurate nitrogen coupling constants in conjugated radical cations is PBE0/N07D//B3LYP/6-31G*, which provides values with a discrepancy smaller than 1.5 G for most of constants. The model has been successfully tested on the calculation of ^{14}N hfccs for different radical cation derivatives of *syn*-1,6:8,13-diimino[14]annulene, which is a highly demanding test because the strong experimental change in the $a_{iso}(^{14}N)$ values critically depends on the local geometry of the diimino fragment which is function of the polymethylene chain length. Furthermore, a whole analysis of the computed structural parameters, NBO and distribution of the spin density of these annulene radicals has allowed to explain the huge increase of the $a_{iso}(^{14}N)$ as well as their stability just for certain polymethylene chain length evidencing the formation of a N-N three electron σ bond.

1. Introduction

Nitrogen conjugated radical cations are labile intermediates involved in an important number of both biological and chemical processes of high interest. Transient nitrogen radical cations are the results of radiation-induced one-electron oxidation reactions of the purine and pyrimidine bases in cellular DNA, that is considered to be the most sensitive cellular target to produce DNA damage leading to the chain breaking.[1-3] Electron Paramagnetic Resonance (EPR) has allowed to detect such radical species from purine and pyrimidine nitrogen bases,[4] contributing to the better understanding of the complex radical chemistry triggered from the primary ionization event. On the other hand, the synthetic potential of amine radical cations is being explored in several new elegant methods to prepare amines with high yields. The ubiquity of amines in bioactive and pharmaceutical compounds has turned the development of efficient synthetic methods into a prolific research field. Among these methods, the photo-redox approach using sunlight stands out, not only because it is an environmental benign methodology but for its efficiency leading to uncommon reaction products.[5-7] Generation of new C-N bond in initial amine **I** (Figure 1), acting as electron-donor under photo-redox conditions, leads to a higher functionalized amine **IV**. The mechanistic studies established that the intermediate formed in a one electron oxidation process is radical cation **II**.[6,8-9] Amine radical cations are capable of initializing multiple downstream pathways, leading to diverse synthetic intermediates such as highly electrophilic iminium ion **III**[7,10-12] which yields amine **IV** by the capture of a nucleophile. Alternatively, amine radical cation **II** can react by disproportionation, yielding nucleophilic α-amino radical **V**.[5,13-15] This neutral radical evolves to iminium ion **III** through one electron oxidation.[15-16]

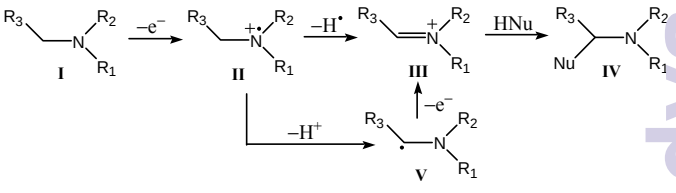

Figure 1. Scheme of amine synthetic photo-redox method.

Intermediate amine radical cation **II**, which is an odd-electron species, is highly reactive. The introduction of aromatic substituents in the initial amine **I** is a useful strategy to lead to a stabilized nitrogen centered radical cation through conjugation,[7,17-18] which produces in better yield the desired amine **IV** by selective nucleophilic attack on the conjugate

Departamento de Química Física Aplicada, Facultad de Ciencias, Universidad Autónoma de Madrid, 28049 Madrid (Spain).
*Corresponding author e-mail: laura.hermosilla@uam.es
Electronic Supplementary Information (ESI) available. See DOI: 10.1039/x0xx00000x

benzylic imine **III**. The presence of the conjugation in the intermediate radical structure makes easier its detection allowing to shed light on the reaction mechanisms that are not always well established.[19-20] Among the available techniques to study radical cations in solution, EPR spectroscopy provides detailed information about the identity of intermediate structures by assignation of the observed isotropic hyperfine coupling constants (a_{iso} or hfccs) to the corresponding nuclei. However, the assignment of the structure based on EPR hfccs of the radical intermediates is not obvious. The ability of the radical cations to evolve to other odd-electron species, by either an intramolecular pathway (e.g., isomerization, transposition, etc.) or by an intermolecular route (as dimerization, hydrogen abstraction …), is a source of misinterpretation of the EPR spectroscopic data leading to mistakes in the mechanistic interpretations. Therefore, a reliable protocol for the assignment of spin densities that enables the correct analysis of the experimental data is essential.

In recent years, density functional theory (DFT) has been successfully applied to the prediction of hfccs of organic radicals.[21] Several benchmark studies[22-37] have tested a wide range of different methodologies, concluding[22-26] that for the nuclei belonging to the three first rows of the Periodic Table the best overall results are obtained when B3LYP[38-39] functional is combined with TZVP[40] or EPR-III[41-42] basis sets. However, the nitrogen nucleus ^{14}N (nuclear spin I = 1) represents an exception. In particular, it was settled for the case of neutral aromatic radicals that the selection of the basis set is of fundamental importance in the prediction of accurate values of nitrogen hfccs.[26,30,43] The number of components of *d* functions plays a key role, so that small basis sets like 6-31G*[44-45] and N07D[27-28] (6 *d* functions) combined with PBE0[46] or B3LYP functionals predict hyperfine constants that are closer to the experimental values than those obtained with larger basis sets with 5 *d* functions. As it is well known, the calculation of accurate values of a_{iso}(^{14}N) in flexible nitroxide radicals presents additional complexity, since effects like vibrational averaging, conformational flexibility and spin delocalization could play a significant role in determining this parameter. In general, static gas-phase quantum mechanical (QM) methods do not lead to very good results, which necessitates more complex computational approaches to provide a reliable description of the radical electronic structure. For instance, it has been shown that an accurate determination of a_{iso}(^{14}N) can be achieved by exploiting a combination of a QM time-independent methodology with molecular mechanics/molecular dynamics (MM/MD) simulations to include vibrational and solvent effects.[29,47-53]

As far as we know, there is not a systematic theoretical study on hfccs of organic conjugated radical cations containing ^{14}N nucleus. This prompted us to benchmark the performance of several functionals and basis sets in the calculation of a_{iso}(^{14}N) of a wide set of conjugated radical cations belonging to a widespread range of chemical families in order to investigate whether the trend observed for cations is the same as for neutral radicals. A set of 50 paramagnetic species containing at least one ^{14}N nucleus with known experimental hfcc has been considered. Calculation of the hfccs is carried out at five different levels of theory, based on their successful presence in the literature concerning hfccs calculation: PBE0/N07D, B3LYP/6-31G*, B3LYP/N07D, B3LYP/TZVP, and B3LYP/EPR-III.

A thorough computational study on radical cations derivatives of *syn*-1,6:8,13-diimino[14]annulene with variable length of the polymethylene chain linking the two N atoms has also been performed in order to explore the large increase of the ^{14}N hfcc with the length of the polymethylene chain together with an increase in the radical cation stability, which makes these species of particular interest.

The main goal of this work is thus to investigate the performance of DFT methodology to obtain accurate values of spin densities of nitrogen conjugated radical cations. The efforts are devoted to the prediction of the values of a_{iso}(^{14}N) which represents the capital challenge searching for the best choice of functional and basis set combination for such a prediction. Besides, it is expected to be a useful tool for EPR spectroscopists, since reliable theoretical values could allow the correct assignment of the experimental isotropic coupling constants, leading to a better understanding of the complex mechanisms in which nitrogen radical cations are involved.

2. Theory and computational details

The isotropic hyperfine coupling constant is related to the spin density at the corresponding nucleus N by:

$$a_{iso}(N) = \frac{\mu_0}{3} g_e g_N \beta_e \beta_N \langle S_z \rangle^{-1} \rho(N) \quad (1)$$

where μ_0 is the permeability of vacuum, g_e is the electronic g factor, g_N is the nuclear g factor of nucleus N, β_e is the Bohr magneton, β_N is the nuclear magneton of nucleus N, $\langle S_z \rangle$ is the mean value of S_z in the electronic state, and $\rho(N)$ is the Fermi contact integral for nucleus N. This later integral is given by

$$\rho(N) = \sum_{\mu\nu} P_{\mu\nu}^{\alpha\beta} \langle \phi_\mu(r) | \delta(r - r_N) | \phi_\nu(r) \rangle \quad (2)$$

$P_{\mu\nu}^{\alpha\beta}$ is an element of the one-electron spin density matrix (the difference between the density matrices for electrons with α and β spins), ϕ are the atomic basis functions, and δ is the Dirac delta operator.

Substituting the corresponding constants in (1), the conversion factors for the different nuclei are given by the expression:

$$a_{iso}(N) = 142.770 \langle S_z \rangle^{-1} g_N \rho(N) \quad (3)$$

where a_{iso} is obtained in Gauss and $\rho(N)$ is expressed in au.

This isotropic term is difficult to compute in quantitative agreement with the experimental data. For this reason, hfccs have received great attention from theoretical chemists since they are very sensitive to errors in the spin density at the nucleus. This fact shows that this property depends on the quality of the wave function employed and the level of calculation used, particularly, the electron correlation, the one-electron basis set, and the molecular geometry.

The set of radical cations investigated in the present work, that is schematically represented in Figure 2, comprises cations of pyrrole derivatives (radicals **1** and **2**, respectively),

dihydrodiazaheterocyclics and their *N*-methyl derivatives (**3**–**16**), heterotricyclics isoelectronically related to the phenalenyl radical and the radical anion of anthracene (**17**–**21**), amino derivatives of ethene and benzene (**22**–**34**), amino derivatives of conjugated hydrocarbons other than benzene (**35**–**39**), dihydropyridazine and phenyl-substituted hydrazines (**40**–**42**), diimino[14]annulenes (**43**–**47**), and diphenyldiazomethane and structurally related compounds (**48**–**50**). Both the radical cation and the trication of the hexaazaoctadecahydrocoronene (**33** and **34**, respectively) have been considered; all the rest are monocations.

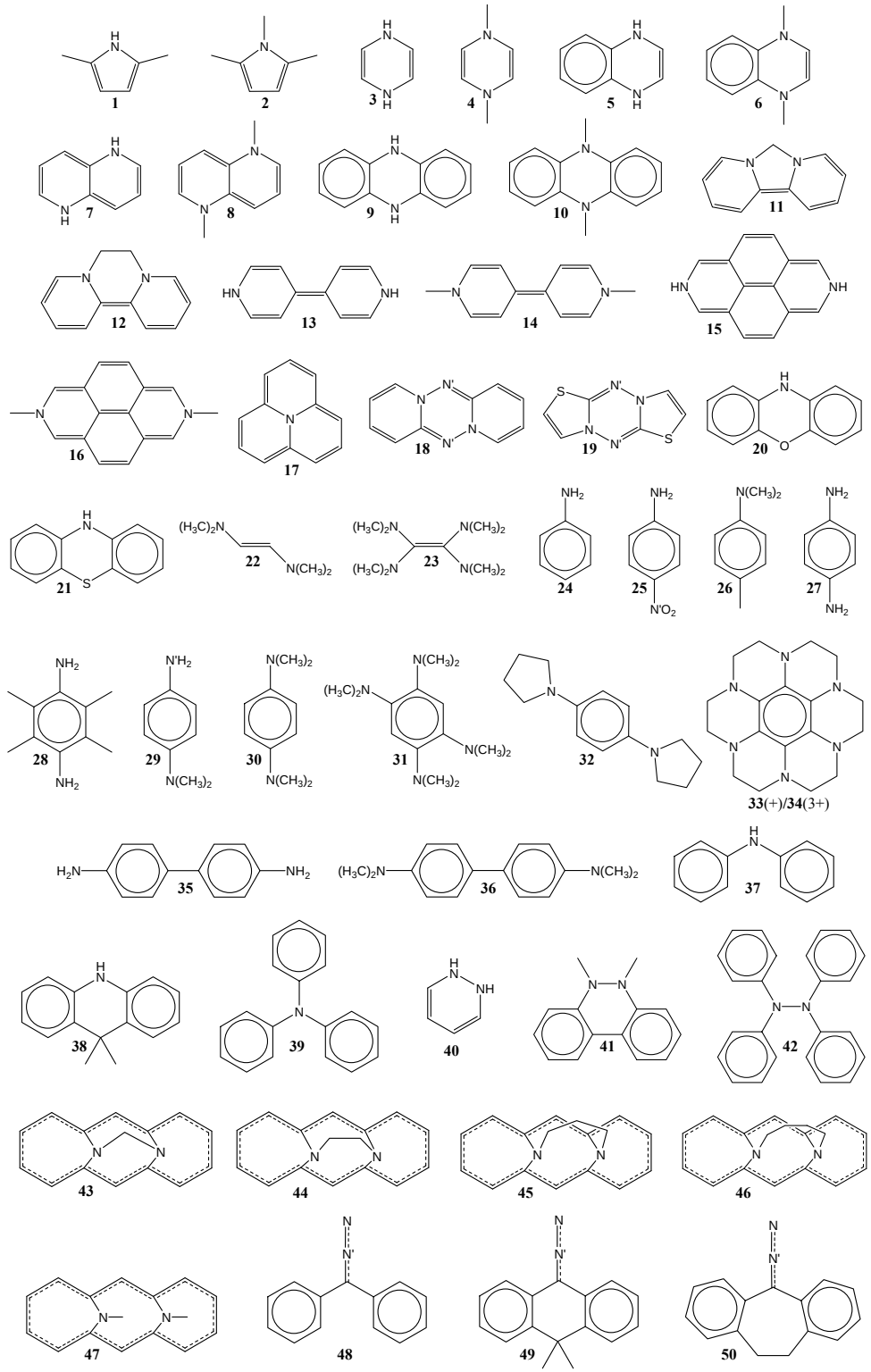

Figure 2. Schematic geometrical structures of the conjugated radical cations.

Molecular geometries of the electronic ground state of each radical were fully optimized at the B3LYP/6-31G* level of theory due to its low computational cost and good results according to previous works.[22-26] Harmonic vibrational frequencies were computed at the same level of theory as the geometry optimization to confirm the nature of the stationary points.

The hfccs of the radicals were evaluated on the optimized structures at five different levels of theory: PBE0/N07D, B3LYP/6-31G*, B3LYP/N07D, B3LYP/TZVP, and B3LYP/EPR-III. N07D is a polarized split-valence basis set developed for the calculation of hfccs with an optimum compromise between reliability and computer time, specifically parameterized for both the PBE0 and the B3LYP functionals.[27-28] The 6-31G* basis set is a small double-ζ basis plus polarization, whereas TZVP and EPR-III are DFT-optimized triple-ζ basis sets. The last one is a larger basis set, including diffuse functions, double *d*-polarizations and a single set of *f*-polarization functions, also optimized for the computation of hfccs by DFT methods.

Natural Bond Orbitals (NBO) were computed on the optimized structures of radicals **43**–**47** at PBE0/N07D and B3LYP/cc-pVTZ[54] levels of theory.

Geometry optimizations and calculation of vibrational frequencies, hfccs and NBO were carried out with the Gaussian09 software package.[55]

Atomic contributions to density deformations of radicals **43**–**47** were computed at B3LYP/cc-pVTZ level of theory on the optimized geometries using DAMQT 2.0 package,[56] with an atomic multipolar expansion of the density up to 10th order. This program uses a method based on the deformed atoms in molecules (DAM) partition,[57-60] which enables to write the molecular density as a sum of pseudoatomic contributions defined with a least deformation criterion.

3. Results and discussion

3.1. Overall performance in modeling hfccs of nitrogen containing conjugated radical cations

The computed hyperfine coupling constants of ^{14}N nuclei obtained for the 50 radical cations are summarized and compared with the experimental values in Table 1. The first column corresponds to the number of each radical in Figure 2. The second column indicates the number of equivalent N atoms. The following five columns report the theoretical hfcc values obtained at the different levels of theory: PBE0/N07D, B3LYP/6-31G*, B3LYP/N07D, B3LYP/TZVP, and B3LYP/EPR-III, all of them carried out on the geometries previously optimized at B3LYP/6-31G*. In the last two columns, the experimental hfccs and their bibliographic references are listed. The experimental a_{iso} are given as absolute values and the sign has been included just in the theoretical data (the sign is not determined directly by EPR experiments; it is assigned on the basis of theoretical results or from double ENDOR or TRIPLE resonance techniques). Nevertheless, comparison of absolute values has been considered henceforth. The hyperfine coupling constants of ^{1}H nuclei have also been computed (provided in Table S1 in the Electronic Supplementary Information (ESI)), being these theoretical values in very good agreement with the experimental values, regardless of the level of theory employed. This result, which is consistent with those obtained in previous works on different types of organic radicals, even on nitrogen containing species,[26] contrasts with that found in the case of ^{14}N hyperfine constants, as explained in detail below. Therefore, only the ^{14}N hfcc data have been considered in the further analysis, although in some cases comparison between both nuclei is performed for completeness.

For each level of theory, a total of 57 $a_{iso}(^{14}N)$ values have been compared with the available experimental data. Radicals **19** and **21**, whose hfccs have not been computed at B3LYP/EPR-III because this basis set is not parameterized for sulfur atom, are an exception.

A first glance at the results collected in Table 1 shows that the experimental $a_{iso}(^{14}N)$ vary from 1.29 to 26.6 G, but most of them are under 10 G. These values are the expected ones for conjugated radicals, in which the spin density is shared with the aromatic π-system. The constants that fall far outside this range (radicals **45**–**47**) will be specifically discussed in section 3.2.

Different factors contribute to the ^{14}N isotropic hyperfine coupling constant magnitude. Firstly, it depends on the pyramidalization at the nitrogen center, in such a way that a non-planar geometry around the N atom tends to increase the $a_{iso}(^{14}N)$. Moreover, in aromatic nitrogen systems, the conjugative effect (interaction between the nitrogen lone pair and the aromatic π system) is crucial. In the case of aniline derivatives, ArNRR', this effect is maximum in general in the planar form (N-R, N-R' bonds coplanar with the aromatic ring) and absent in the perpendicular one (N-R, N-R' bonds orthogonal to the aromatic ring). In the derivatives with the *ortho* substituents on the aromatic ring, the steric interaction of R and R' groups on the nitrogen has the opposite effect, being higher in the planar form than in the perpendicular one. The most stable radical conformation would be the result from a balance between these opposite factors. On the other hand, the effect of a *para* ring substituent depends on the electron donating or electron withdrawing character. On the basis of these substantial considerations, we analyzed the values of the nitrogen hyperfine coupling constants of the studied radicals, and the performance of the different methods/basis sets to model these magnetic parameters.

Table 1. Theoretical hyperfine coupling constants (G) of ^{14}N nucleus of the conjugated radical cations at the following levels: PBE0/N07D, B3LYP/6-31G*, B3LYP/N07D, B3LYP/TZVP, and B3LYP/EPR-III. All calculations were carried out on the geometries optimized at B3LYP/6-31G*.

		a_{iso} (theoretical)						
		PBE0	B3LYP				experimental	
no.	nuclei	N07D	6-31G*	N07D	TZVP	EPR-III	a_{iso}	ref
1	N	–3.9	–3.2	–3.5	–3.5	–3.4	4.0	[61-62]
2	N	–4.2	–3.3	–3.6	–3.6	–3.5	4.2	[62]
3	2N	+6.9	+6.7	+6.5	+4.8	+5.4	7.40	[63]
4	2N	+8.4	+7.7	+7.7	+6.0	+6.6	8.36	[64]
5	2N	+6.3	+6.0	+5.8	+4.4	+4.9	6.65	[63]
6	2N	+7.5	+6.7	+6.8	+5.2	+5.8	7.42	[65]
7	2N	+2.7	+2.6	+2.6	+1.9	+2.2	2.86	[66]
8	2N	+3.5	+3.2	+3.2	+2.4	+2.7	3.40	[66]
9	2N	+5.6	+5.3	+5.2	+3.9	+4.4	6.12	[63]
10	2N	+6.7	+5.9	+6.1	+4.7	+5.2	6.86	[67]
11	2N	+4.2	+3.7	+3.8	+2.9	+3.2	4.34	[68]
12	2N	+4.0	+3.6	+3.6	+2.7	+3.1	4.08	[69]
13	2N	+3.4	+3.3	+3.7	+2.4	+2.7	3.56	[63]
14	2N	+4.4	+4.0	+4.0	+3.1	+3.4	4.23	[70]
15	2N	+3.9	+3.8	+3.6	+2.7	+3.1	4.04	[71]
16	2N	+5.0	+4.5	+4.6	+3.5	+3.9	4.70	[71]
17	N	+1.8	+1.2	+1.2	+1.1	+1.1	1.29	[72]
18	2N	+2.8	+2.4	+2.4	+1.6	+1.9	2.80	[73]
	2N’	+7.4	+7.0	+6.9	+4.9	+5.6	6.18	
19	2N	+4.1	+3.7	+3.7	+2.7	[a]	4.00	[73]
	2N’	+6.7	+6.3	+6.3	+4.5	[a]	5.96	
20	N	+6.9	+6.4	+6.3	+4.8	+5.3	7.83	[74]
21	N	+5.8	+5.5	+5.3	+4.0	[a]	6.41	[74]
22	2N	+8.1	+7.5	+7.5	+5.8	+6.4	6.95	[75]
23	4N	+4.6	+4.6	+4.4	+3.7	+3.9	4.90	[75]
24	N	+6.7	+6.8	+6.3	+4.7	+5.3	7.68	[76]
25	N	+6.8	+6.8	+6.4	+4.8	+5.3	8.01	[76]
	N’	–2.0	–1.6	–1.7	–1.8	–1.7	2.06[b]	
26	N	+10.7	+9.7	+9.7	+7.6	+8.3	11.17	[77]
27	2N	+4.7	+4.9	+4.5	+3.3	+3.7	5.29	[78]
28	2N	+3.9	+4.2	+3.7	+2.7	+3.0	4.72	[79]
29	N	+8.2	+7.4	+7.4	+5.8	+6.4	7.62	[77]
	N’	+4.0	+4.3	+3.9	+2.8	+3.2	4.73	
30	2N	+7.1	+6.5	+6.5	+5.1	+5.6	7.02	[80]
31	4N	+4.3	+4.0	+4.1	+3.4	+3.6	3.57	[81]
32	2N	+7.1	+6.5	+6.5	+5.1	+5.6	6.82	[82]
33	6N	+2.5	+2.3	+2.3	+1.8	+2.0	2.60	[83]
34	6N	+2.6	+2.4	+2.4	+1.8	+2.0	2.81	[83]
35	2N	+3.0	+3.2	+2.9	+2.1	+2.4	3.60	[84]
36	2N	+5.0	+4.5	+4.5	+3.5	+3.9	4.88	[84]
37	N	+8.5	+7.7	+7.6	+5.9	+6.5	9.03	[85]
38	N	+8.0	+7.3	+7.3	+5.6	+6.2	8.56	[85]

39	N	+9.9	+8.8	+8.8	+6.9	+7.6	10.19	[85]
40	2N	+7.3	+7.1	+6.9	+5.3	+5.9	7.81	[86]
41	2N	+8.0	+7.3	+7.3	+5.6	+6.2	8.79	[87]
42	2N	+6.5	+6.0	+5.9	+4.5	+5.0	7.52	[88]
43	2N	+7.2	+6.8	+7.0	+6.1	+6.4	6.33	[89]
44	2N	+6.4	+6.2	+6.3	+5.3	+5.6	6.11	[89]
45	2N	+15.5	+13.9	+14.6	+12.6	+13.4	16.85	[89-90]
46	2N	+23.2	+21.0	+22.4	+20.9	+21.4	25.7	[89,91]
47	2N	+25.1	+22.8	+24.4	+22.9	+23.4	26.6	[89]
48	N	+4.5	+4.1	+4.6	+2.6	+3.4	4.4	[92]
	N’	–3.9	–2.7	–3.2	–3.6	–3.4	3.3	
49	N	+4.6	+4.3	+4.7	+2.7	+3.5	4.0	[92]
	N’	–3.2	–2.2	–2.5	–3.1	–2.8	3.2	
50	N	+4.1	+3.8	+4.2	+2.3	+3.1	4.4	[92]
	N’	–3.2	–2.2	–2.5	–3.0	–2.8	3.8	

[a]EPR-III basis set is not parameterized for third row nuclei. [b]Experimental datum was assigned with opposite sign.[76,93]

The increase in the $a_{iso}(^{14}N)$ values observed in the substitution of protons at the N atom by methyl group in couples of radicals **1** *vs* **2**, **3** *vs* **4**, **5** *vs* **6**, **7** *vs* **8**, **9** *vs* **10**, **13** *vs* **14**, **15** *vs* **16**, **27** *vs* **29**, **29** *vs* **30**, and **35** *vs* **36** is well reproduced in the calculation scheme. The calculated geometry shows a slight pyramidalization when replacing hydrogen atom by methyl group in some of these cases (the out of plane dihedral angle reaches a maximum value of 2.5º), but not in all of them. Therefore, the increase in electron density cannot be attributed only to this effect. The electron donation by inductive effect of the methyl group seems to be the main responsible of the observed increase. This result is reinforced when we analyze the couples of radicals **27** *vs* **29**, **29** *vs* **30**, and **35** *vs* **36**, which show the greater differences in hfccs, and wherein substitution of two H atoms by methyl groups has been made. A similar enhance in $a_{iso}(^{14}N)$ is found when protons at the N atom are replaced by a phenyl ring (compare radicals **24**, **37** and **39**), pointing out the electron donation effect of this group by resonance.

As expected, the nitrogen coupling constant decreases with expansion of the π-system (see, for instance, couples of radicals **3** *vs* **5**, **4** *vs* **6**, **5** *vs* **9**, and **6** *vs* **10**) and/or introduction of a second amino group (radicals **24** and **27**), a result also reproduced by the computational models.

The series of radical cations **43**–**47** constitutes an special case in which the $a_{iso}(^{14}N)$ increases greatly with the length of the polymethylene chain linking the N atoms, increase closely reproduced by the theoretical calculation schemes. A detailed analysis provided by the model, linking the experimental attributes with structural features, is displayed in the next section.

Both σ and π structures have been experimentally observed for the radical cation of diphenyldiazomethane (**48**) and its structurally related **50** but, to our knowledge, only the π system has been detected for the radical cation **49**.[92-93] The π-radical cations are expected to have a linear CNN group which should be bent in their σ counterparts. It has been found[92] that the structure of radical **48** only depends on experimental conditions, which indicates that both states are energetically very close. Nevertheless, previous theoretical calculations,[92] and those carried out in the present work indicate that the π structure is more stable in the three cations **48**–**50**. Thus, only this one has been considered in the present study leading to obtaining calculated hfccs values that are quite close to the experimental ones.

A thorough analysis of data in Table 1 indicates that PBE0/N07D, B3LYP/6-31G*, and B3LYP/N07D levels reproduce with accuracy the values of the experimental ^{14}N hfcc, whereas B3LYP/TZVP and B3LYP/EPR-III combinations tend to underestimate this constant in a great amount, specially that of the TZVP basis set. Taking into account that both the N07D and 6-31G* basis sets are smaller, and therefore more computationally economical, the combinations with TZVP and EPR-III are not recommended for this kind of calculations.

In order to better analyze the results, the calculated *vs* experimental a_{iso} of ^{14}N nuclei for the 50 species are plotted in Figure 3, at the three more reliable calculation levels. We have considered in the further analysis only the hfcc data obtained with N07D and 6-31G* basis sets, although all the data obtained at the five calculation levels are displayed in Figure S1 in the ESI. The range 0 – 10 G is represented in Figure 3 for clarity, since most of the data lie in this range, as previously exposed (plot of the whole range is shown in Figure S1 in the ESI). Figure 3 clearly shows that the representation of calculated against experimental hfccs shows a linear dependence (fits are plotted as solid lines, see below). Good performance in the prediction of ^{14}N coupling constant is found for the three levels of theory, with no large dispersion nor major discrepancies in any of the data in general. Roughly, theoretical calculations tend to underestimate the values of $a_{iso}(^{14}N)$, the decrease being smaller in the case of PBE0/N07D level of theory than in the two other cases.

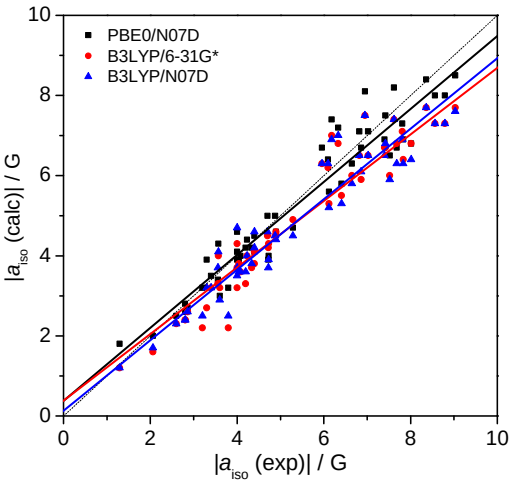

Figure 3. Plot of theoretical *vs* experimental $a_{iso}(^{14}N)$ of the conjugated radical cations in the range 0 – 10 G, calculated at PBE0/N07D (■), B3LYP/6-31G* (●), and B3LYP/N07D (▲) levels of theory. Linear fits are represented by solid lines.

Representation of calculated *vs* experimental $a_{iso}(^{1}H)$ at the five calculation levels are also provided in Figure S2 in the ESI for comparison. As previously indicated, all the five levels of theory estimate $a_{iso}(^{1}H)$ in very good agreement with the experimental data, and there is not much discrepancy among the results obtained with the different basis sets.

Additional information can be extracted from the analysis of the absolute ($|a_{iso,calc}|-|a_{iso,exp}|$) and relative ($(|a_{iso,calc}|-|a_{iso,exp}|)/|a_{iso,exp}|$) deviations of the calculated $a_{iso}(^{14}N)$ compared to the corresponding experimental data. Figure 4 shows these results for the three more reliable levels of theory, although comparison of all the five calculation levels is displayed in Figure S3 in the ESI. As a general trend, it is possible to point out that PBE0/N07D yields predictions in better agreement to the experimental than the other two computational schemes. The vast majority of the data has a discrepancy lower than 1.5 G. Radicals **45**–**47** are the exceptions, as their relative deviations are much higher, especially in the case of B3LYP/N07D and B3LYP/6-31G* levels of theory. The explanation is that their hfccs are much larger (16.85 – 26.6 G), so it is acceptable a discrepancy of 3 – 5 G. In fact, the relative deviations (bottom of Figure 4), which are more meaningful, are not very large in the case of these three radicals, but are within a range of around 20%, as most of the rest of data. In this part of this Figure 4, three outliners which correspond to radicals **17**, **49** (N') and **50** (N') attract attention because of their larger differences. Contrary to the previous case, small hfcc values with a small absolute difference lead to a large relative error.

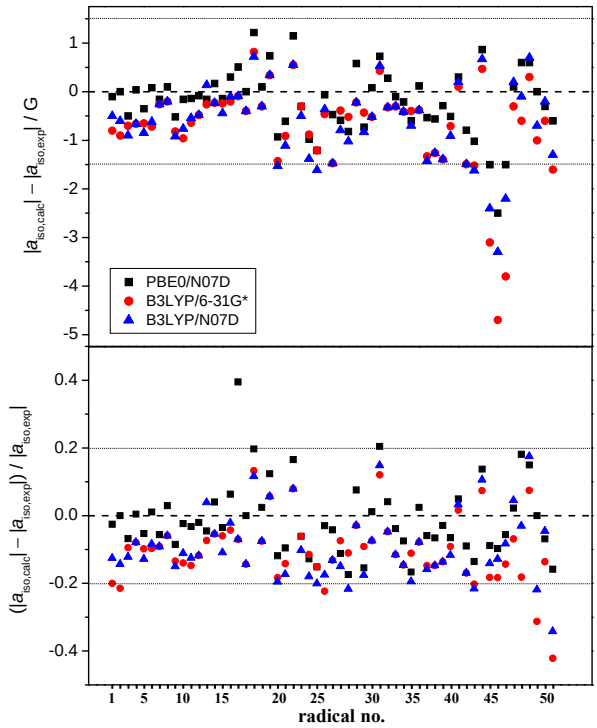

Figure 4. Absolute (top) and relative (bottom) deviation of the calculated $a_{iso}(^{14}N)$ of the conjugated radical cations computed at PBE0/N07D (■), B3LYP/6-31G* (●), and B3LYP/N07D (▲) levels of theory.

While Figures 3 and 4 give a broad overview for the three more reliable computational protocols, we have also carried out a closer inspection of the results by means of a statistical analysis of all the five levels included in Table 1. The number of data is high enough to extract general conclusions as regards the prediction of ^{14}N hfccs on conjugated radical cations. The results for the linear regression analysis for the computation of this parameter over the five sets of data are given in Table 2. The corresponding linear fits are represented by solid lines in Figure 3, and Figures S1 and S2 in the ESI (regression lines of plots in the range 0 – 10 G are also those corresponding to the linear fits of all data points). Statistics of calculated values are based on different parameters of the regression analysis: intercept, slope, correlation coefficient (R^2) of the least-squares fit, as well as the number of data (N), range (minimum and maximum absolute values), maximum absolute error, mean absolute deviation (MAD), and the ratio range/MAD.

A similar regression analysis was also carried out for ^{1}H nuclei. The statistical parameters are summarized in Table S2 in the ESI.

Table 2. Regression analysis for predictions of ^{14}N hfccs (G).

Level of theory	intercept	slope	R^2	N	|min|	|max|	max. absolute error	MAD[a]	range/MAD
PBE0/N07D	0.3795	0.9103	0.9850	57	1.8	25.1	2.5	0.50	46.60
B3LYP/6-31G*	0.3857	0.8303	0.9822	57	1.2	22.8	4.7	0.82	26.34
B3LYP/N07D	0.1371	0.8794	0.9825	57	1.2	24.4	3.3	0.78	29.74
B3LYP/TZVP	–0.5771	0.8125	0.9671	57	1.1	22.9	4.8	1.80	12.11
B3LYP/EPR-III	–0.3302	0.8368	0.9795	54	1.1	23.4	4.3	1.43	15.59

[a] MAD (Mean Absolute Deviation) = $\frac{1}{N}\sum_{i}^{N}\left|a_{iso}(calc)-a_{iso}(exp)\right|$.

A first conclusion that is worth to stress as regards of Table 2 is that, as mentioned above, TZVP and EPR-III basis sets with the B3LYP hybrid functional yield results worse than those predicted with the smaller split-valence 6-31G* and N07D basis sets with either B3LYP or PBE0 functionals. All the parameters of the regression analysis support this result: they have the poorest correlation coefficients, slopes and range/MAD ratios, as well as higher values of mean absolute deviations. As found in previous works on neutral aromatic radicals,[26-28] the number of components of *d* functions seems to be of fundamental importance in the calculation of $a_{iso}(^{14}N)$ of conjugated radical cations as well, and the additional *s* function implicitly added when using a 6 *d* set (in 6-31G* and N07D basis sets) plays a non-negligible role in completing the *s* space, and thus in obtaining more accurate hfccs in spite of the smaller size.

The correlation coefficient of the three more reliable calculations (those of 6-31G* and N07D basis sets) are very high (>0.98), that of the PBE0/N07D level being slightly larger. Consequently, any of them is expected to predict values with no high scattering, in concordance with what is observed in Figures 3 and 4.

The slopes of the least-squares fits for B3LYP/6-31G* and B3LYP/N07D computations, although not bad, are not so close to the unity as that of PBE0/N07D. Given that intercepts in all the three cases are quite close to zero (<0.39 G), it is possible to conclude that values provided by the latter combination correlate to the experimental data better than the rest. Since the intercepts are close to zero, larger the slope further away the calculated values are from the experimental, being the differences among the levels of theory as noticeable as higher is the magnitude of the hfcc (see Figure S1 in the ESI).

As expected, all the rest of the regression parameters are also in accordance with the fact that PBE0/N07D level of theory is preferred to predict ^{14}N hfcc of this kind of species. It has the lower error and MAD as well as much larger range/MAD ratio, which is the most representative parameter to take into account for the relative comparison of the accuracy of the different methodologies.

It is important to stress that computed values of $a_{iso}(^{14}N)$ at PBE0/N07D level of theory using only the static gas-phase optimized structures of the radical cations are in very good agreement with the experimental data. It is well known that calculation of accurate values of ^{14}N hfcc usually requires inclusion of factors like vibrational averaging, conformational flexibility and/or environmental effects, by means of more complex integrated strategies. For instance, several cases of flexible nitroxide-type radicals have been studied in depth by using this kind of approaches, including molecular dynamics simulations with *ad hoc* force fields combined with time-independent calculations of vibrational averaging effects.[29,47-53] The very good predictions obtained in the case of conjugated radical cations with static gas-phase calculation at PBE0/N07D//B3LYP/6-31G* level suggest that, presumably, conjugation constrains the flexibility of the molecular structures, so that environmental and/or vibrational effects would not play a significant role in determining this parameter. This is a very important finding because the computation model provides a general reliable tool to interpret the experimental data without further sophisticated calculations.

3.2. Modeling hfccs of derivatives of *syn*-1,6:8,13-diimino[14]annulene radical cations

As previously mentioned, we have devoted special attention to the family of radical cations **43**–**47**, derivatives of *syn*-1,6:8,13-diimino[14]annulene, in which the two N atoms are linked by a polymethylene chain, $-(CH_2)_n-$ (n = 1 – 4 correspond to cation radicals **43**–**46**, respectively), and the radical cation of N,N'-dimethyl-*syn*-1,6:8,13-diimino[14]annulene, radical **47**. In this family, a large range in the experimental values[89-91] of the hfccs for the nitrogen nuclei was observed, going from 6.33 G for radical **43** to 25.7 G for radical **46**, that is, an increase of around 20 G when the chain goes from n = 1 to n = 4. Radical cation **47**, that could be considered as having a very long polymethylene chain joining the N atoms, shows larger $a_{iso}(^{14}N)$ value (26.6 G). In radicals **45** and **46**, the high experimental $a_{iso}(^{14}N)$ value is accomplished by a spectacular increase in the radical cation stability, allowing crystalization.[89-91,93] Perchlorate salt of radical cation **47** was also isolated but not sufficiently stable for an X-ray crystallographic structure analysis.[89] The high thermodynamic and kinetic stability, as well as the size of the ^{14}N coupling constants, which is unusually large for a π-radical cation extending over 14 C atoms, strongly suggest that **45**–**47** radical cations are N-centered paramagnetic species with a N-N intramolecular three electron σ bond. The bond formation has been supported by the shortening of the N-N distance, determined by X-ray crystallography, in **45** (2.160 Å) and **46** (2.189 Å) radical cations with respect to the neutral molecules (2.705 and 2.560 Å, respectively). However, formation of such a bond could not take place in radicals **43** and **44** due to the relative orientation of the N lone pairs driven by the short

chain.[89-91,93-94] In order to study the nature of the N-N interaction, the theoretical data obtained from the DFT calculations were analyzed in depth and compared to the experimental data. Table 3 lists the structural parameters (N-N distance, C-N-C bond angle, and C_{ring}-C_{ring}-C_{bridge}-N torsion angle) of the B3LYP/6-31G* optimized geometries of radicals **43**–**47**, together with the available experimental data determined by X-ray crystallographic structure analysis. The calculations closely reproduce the experimental distances and angles of radicals **45** and **46**, and clearly show the shortening of the N-N distance when passing from radical cation **44** (2.462 Å) to **45** (2.190 Å), which is indicative of an onset of a bonding interaction between the two N atoms. Moreover, the averaged torsion angle ϕ, which indicates the degree of pyramidalization of the N atoms, also points out in the direction of a different behaviour when the polymethylene chain rises $n > 2$. The change of the sign of such an out-of-plane angle indicates that the nitrogen atoms are positioned at different sides of the plain defined by the C atoms, as can be clearly seen in Figure 5 where optimized geometries of radicals **43**–**47** are schematically represented. The shortening of the N-N distance and the change in the arrangement seem to be crucial in the type of the interaction between the two nitrogen atoms.

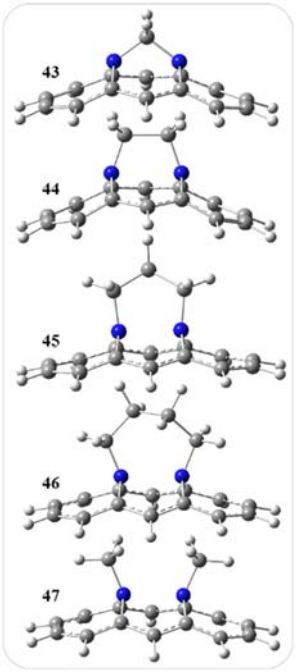

Figure 5. Schematic representation of the optimized geometries of radicals **43**–**47** at B3LYP/6-31G* level of theory.

Table 3. Theoretical structural parameters of radicals **43**–**47** at B3LYP/6-31G* level of theory. Available experimental data determined by X-ray crystallography in parenthesis.

Radical no.	N-N distance / Å	χ bond angle[a,b] / º	ϕ torsion angle[a,c] / º
43	2.296	112.7	–29.2
44	2.462	118.7	–12.9
45	2.190 (2.160[d])	119.2 (119.1[d])	10.4
46	2.249 (2.189[e])	117.1 (116.7[e])	19.9
47	2.236	116.7	21.0

[a]Averaged values. [b]χ is the bond angle C-N-C. [c]ϕ is the out-of-plane dihedral angle C_{ring}-C_{ring}-C_{bridge}-N. [d]From ref 90. [e]From ref 91.

In order to settle the nature of the N-N intramolecular interaction, natural bond orbitals (NBO) analysis was also carried out at PBE0/N07D and B3LYP/cc-pVTZ levels of theory on the previously optimized structures of paramagnetic species **43**–**47**. Both combinations lead to qualitatively similar results, so only results at B3LYP/cc-pVTZ are analyzed henceforth. Figure 6 depicts the localization of the involved NBO of radicals **44** and **45**. Orbitals of the N atoms in radical **44** are of the lone pair type (occupancy between $0.75e$ – $0.94e$). They have more than 97% *p*-character and no interaction between the nitrogen atoms. A different scenario is found in radical **45**, since apart from two lone pair type NBO (occupancy $0.96e$), a σ(N-N) orbital arises, which is consistent with the formation of a N-N three electron σ bond. NBO analysis of radical cations **43**, **46** and **47** (provided in Figure S4 in the ESI) indicates the absence of such a bond in the first radical and the presence in the last two. This result agrees with the experimental findings. The remaining results explained below also point out a similar behaviour between radicals **43** and **44**, and among cations **45**–**47**, so that radicals **44** and **45** have been chosen as representative cases of absence and presence, respectively, of N-N three electron σ bond henceforth. As can be observed in Figure 6 (and Figure S4 in the ESI), the relative orientation of the lone pairs is slightly different in the two groups due to the driving force of the connecting chains. The small size of the groups linking the two N atoms in radicals **43** and **44** forces the lone pairs to be oriented away from the facing nitrogen atoms, avoiding the formation of a bond. By contrast, a longer polymethylene chain allows the lone pairs to be directed toward each other, leading to the formation of the N-N three electron σ bond.

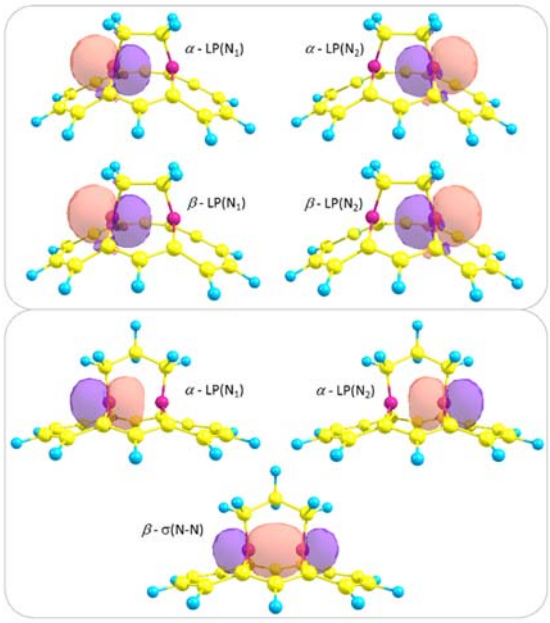

Figure 6. Plot of selected NBO of radicals **44** (top) and **45** (bottom), computed at B3LYP/cc-pVTZ//B3LYP/6-31G* level of theory.

Electron density of radicals **43**–**47** was also computed at B3LYP/cc-pVTZ level of theory using DAMQT 2.0 package, with an atomic multipolar expansion of the density up to 10th order. In Figure 7, the N atomic contributions to the positive density deformations (charge accumulation) of the radical cations **44** and **45** has been plotted at the contour level of 0.001 a.u. (results for radicals **43**, **46** and **47** are provided in Figure S5 in the ESI). It can be clearly seen the lack of density between the nitrogen atoms in radicals **43** and **44**, while the contribution in the internuclear region is large in radicals **45**–**47**, in full agreement with the NBO analysis and the experimental results.

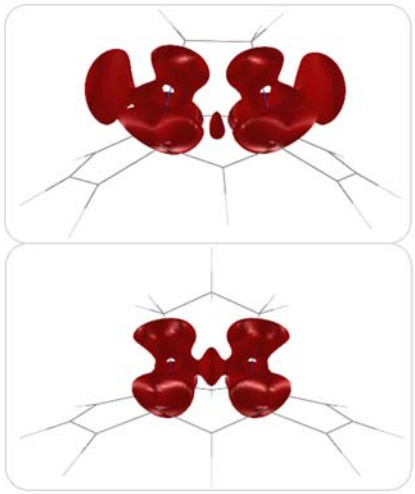

Figure 7. Plot of N atomic contributions to positive density deformations (contour = 0.001 a.u.) of radicals **44** (top) and **45** (bottom), computed at B3LYP/cc-pVTZ//B3LYP/6-31G* level of theory.

The accommodation of almost the entire spin population in the nitrogen orbitals participating in the three electron σ bond lead to the large $a_{iso}(^{14}N)$ values observed for radicals **45**–**47**, if compared to those of species **43** and **44** where the spin population is expected to be shared with the aromatic π-system. As shown in Figure 8 (and Figure S6 in the ESI), plot of spin densities clearly supports this issue, since the spin population is almost completely located in the N atoms in radicals **45**–**47**, whereas it is more delocalized onto the ring in radicals **43** and **44**. However, the differences in the nitrogen hfcc values by the increase of a methylene unit going from cation **45** to **46** is not explained in terms of spin population because in both radicals the population is located entirely in the N-N bond. The explanation has to be found in the pyramidalization of the N atoms that increases the *s* character of the orbitals accommodating the odd electron and thus causing the observed rise of the ^{14}N coupling constant in radical **46** related to **45**. The decrease in the C-N-C bond angle (χ, listed in Table 3) from a value very close to 120º for radical cation **45** (corresponding to sp^2 hybridization at the nitrogen atom) to ~117º for radical **46**, and the increase in the nitrogen out-of-plane ϕ from ~10º to ~20º, clearly point to the rise of the *s* character in the N AOs participating at the N-N bond that moves from sp^2 into the direction of sp^3 hybridization, and therefore rationalizes the observed increase of the ^{14}N coupling constants with decreasing angle χ. Radical **47** shows also a very large experimental $a_{iso}(^{14}N)$ value, even slightly larger than that observed for cation **46** (26.6 versus 25.7 G). Moreover, this radical cation has been described as very stable,[89] although no crystallographic data are available. Our model predicts for radical **47** a N-N distance slightly lower and also a pyramidalization degree of the N atoms slightly greater than radical **46**, as it is displayed in Table 3, supporting the experimental features observed for this radical.

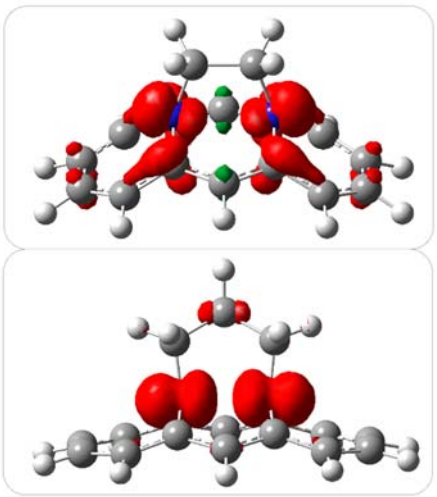

Figure 8. Plot of spin densities (contour = 0.005 a.u.) of radicals **44** (top) and **45** (bottom), computed at PBE0/N07D//B3LYP/6-31G* level of theory.

Plot of computed $a_{iso}(^{14}N)$ values for radicals **45**–**47** versus C-N-C bond angle results in an almost perfect straight line, as shown in Figure 9. Linear dependence has been previously[91] pointed out for the set of experimental data including radical cations **45**, **46** and also 1,6-diazabicyclo[4.4.4]tetradecane radical cation, with a regression line also represented in Figure 9. Agreement between both fit lines is evident, which is another proof of the good performance of the theoretical model proposed in this paper.

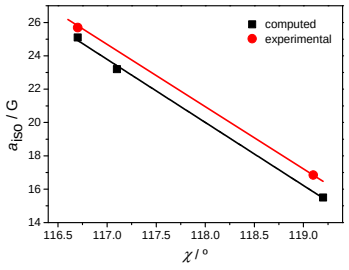

Figure 9. Plot of computed data (PBE0/N07D//B3LYP/6-31G*) of $a_{iso}(^{14}N)$ versus C-N-C bond angle χ for radicals **45**–**47** (■), and experimental data[90-91] of radicals **45** and **46** (●). Linear fits are represented by solid lines. Regression line of experimental data includes 1,6-diazabicyclo[4.4.4]tetradecane.[91]

Conclusions

The performance of several functionals and basis sets in the calculation of isotropic hyperfine coupling constants of a wide set of organic conjugated radical cations has been analyzed by comparing experimental data, 57 $a_{iso}(^{14}N)$ and 165 $a_{iso}(^{1}H)$, to the corresponding computational values obtained from calculations at five different levels of theory: PBE0/N07D, B3LYP/6-31G*, B3LYP/N07D, B3LYP/TZVP, and B3LYP/EPR-III.

As in previous works on nitrogen containing radicals, the prediction of $a_{iso}(^{1}H)$ is in very good agreement with the experimental data whatever combination is used, although significant differences are found in the case of $a_{iso}(^{14}N)$. A thorough comparison of the results by means of regression analysis shows that the five levels of theory are able to predict reliable values of $a_{iso}(^{1}H)$, B3LYP/TZVP combination being slightly advisable. A similar investigation on ^{14}N hfccs clearly indicates that B3LYP/TZVP and B3LYP/EPR-III methodologies are not adequate for such calculation, since smaller basis sets like 6-31G* or N07D provide $a_{iso}(^{14}N)$ values closer to the experimental ones. Therefore, it is possible to establish that in the case of organic conjugated radical cations the selection of the basis set is also of fundamental importance for the prediction of accurate values of nitrogen hfccs (the number of components of *d* functions is 6 for 6-31G* and N07D basis sets whereas it is 5 for TZVP and EPR-III basis sets).

As a final summary, for calculating with accuracy $a_{iso}(^{14}N)$ of conjugated radical cations, we recommend using PBE0 functional in conjunction with the N07D basis set, a combination that was in fact specifically developed for the calculation of hfccs of second- and third- row nuclei with an optimum compromise between reliability and computer time. These calculations at PBE0/N07D//B3LYP/6-31G* level of theory provide very good predictions without the necessity of resort to more complex calculations including solvent effects and/or vibrational contributions.

An in depth investigation has been carried out on radical cations derivatives of *syn*-1,6:8,13-diimino[14]annulene, in which the two N atoms are linked by a polymethylene chain with variable number of methylene units from 1 to 4, as well as the radical cation of N,N'-dimethyl-*syn*-1,6:8,13-diimino[14]annulene. The great rise of the $a_{iso}(^{14}N)$ with the length of the polymethylene chain experimentally observed, together with an increase in the radical cation stability makes this series of particular interest. Analysis of the computed structural parameters, NBO, and distribution of the spin density have allowed to reproduce the available experimental structural data, account for the great rise of the $a_{iso}(^{14}N)$ with the length of the polymethylene chain, and explain the different stability of radicals along the annulene series on the basis of the formation of a N-N intramolecular three electron σ bond, supporting the quality of the model here displayed.

Therefore, the proposed computational model is expected to result in an important tool, increasing the experimentalists' ability to correctly assign the EPR spectra of structurally uncertain radicals.

Acknowledgements

The Spanish Ministry is gratefully acknowledged for financial support (MAT2011-29174-C02-02).

References

1 S. Steenken, *Chem. Rev.* 1989, **89**, 503-520.
2 S. Kanvah, J. Joseph, G. B. Schuster, R. N. Barnett, C. L. Cleveland, U. Landman, *Acc. Chem. Res.* 2010, **43**, 280-287.
3 J. Cadet, J. R. Wagner, V. Shafirovich, N. E. Geacintov, *Int. J. Radiat. Biol.* 2014, **90**, 423-432.
4 R. A. Spalletta, W. A. Bernhard, *Radiat. Res.* 1993, **133**, 143-150.
5 N. Hoffmann, *Pure Appl. Chem.* 2007, **11**, 1949-1968.
6 J. Hu, J. Wang, T. H. Nguyen, N. Zheng, *Beilstein J. Org. Chem.* 2013, **9**, 1977-2001.
7 A. G. Condie, J. C. González-Gómez, C. R. J. Stephenson, *J. Am. Chem. Soc.*, 2010, **132**, 1464-1465.
8 L. Shi, W. Xia, *Chem. Soc. Rev.* 2012, **41**, 7687-7697.
9 S. Maity, N. Zheng. *Synlett.* 2012, **23**, 1851-1856.
10 C.-J. Li, *Acc. Chem. Res.* 2009, **42**, 335-344.
11 S.-I. Murahashi, D. Zhang, *Chem. Soc. Rev.* 2008, **37**, 1490-1501.
12 A. K. Yadav, L. D. S. Yadav, *Tetrahedron Lett.* 2015, **5** 686-689.
13 A. Mac Nally, C. K. Prier, D. W. C. Mac Millan, *Science*, 2011, **334**, 1114-1117.
14 Y. Miyake, K. Nakajima, Y. Nishibayashi, *Chem. Eur. J.* 2012, **18**, 16473-16477.
15 P. Kohls, D. Jadhav, G. Pandey, O. Reiser, *Org. Lett.* 201 **14**, 672-675.
16 M. Rueping, C. Vila, R. M. Koenigs, K. Poscherny, D. C Fabry, *Chem. Commun.* 2011, **47**, 2360-2362.

17 C. Min, A. Sanchawala, D. Seidel, *Org. Lett.* 2014, **16**, 2756-2759.
18 C. K. Prier, D. W. C. Mac Millan, *Chem. Sci.* 2014, **5**, 4173-4178.
19 M. Rueping, S. Zhu, R. M. Koenigs, *Chem. Commun.* 2011, **47**, 12709-12711.
20 D. B. Freeman, L. Furst, A. G. Condie, C. R. J. Stephenson, *Org. Lett.* 2012, **14**, 94-97.
21 M. L. Munzarová, DFT Calculations of EPR Hyperfine Coupling Tensors. In *Calculation of NMR and EPR Parameters: Theory and Applications*; M. Kaupp, M. Bühl, V. G. Malkin, Eds.; Wiley-VCH: Weinheim, Germany, 2004; pp 463-482.
22 L. Hermosilla, P. Calle, J. M. García de la Vega, C. Sieiro, *J. Phys. Chem. A* 2005, **109**, 1114-1124.
23 L. Hermosilla, P. Calle, C. Sieiro, *Phosphorus Sulfur Silicon Relat. Elem.* 2005, **180**, 1421-1422.
24 L. Hermosilla, P. Calle, J. M. García de la Vega, C. Sieiro, *J. Phys. Chem. A* 2005, **109**, 7626-7635.
25 L. Hermosilla, P. Calle, J. M. García de la Vega, C. Sieiro, *J. Phys. Chem. A* 2006, **110**, 13600-13608.
26 L. Hermosilla, J. M. García de la Vega, C. Sieiro, P. Calle, *J. Chem. Theory Comput.* 2011, **7**, 169-179.
27 V. Barone, P. Cimino, *Chem. Phys. Lett.* 2008, **454**, 139-143.
28 V. Barone, P. Cimino, E. Stendardo, *J. Chem. Theory Comput.* 2008, **4**, 751-764.
29 R. Improta, V. Barone, *Chem. Rev.* 2004, **104 (3)**, 1231-1254.
30 P. Stipa, *Chem. Phys.* 2006, **323**, 501-510.
31 A. Rogowska, S. Kuhl, R. Schneider, A. Walcarius, B. Champagne, *Phys. Chem. Chem. Phys.* 2007, **9**, 828-836.
32 R. Amorati, G. F. Pedulli, M. Guerra, *Org. Biomol. Chem.* 2010, **8**, 3136-3141.
33 X. Chen, Z. Rinkevicius, Z. Cao, K. Ruud, H. Ågren, *Phys. Chem. Chem. Phys.* 2011, **13**, 696-707.
34 J. Autschbach, S. Patchkovskii, B. Pritchard, *J. Chem. Theory Comput.* 2011, **7**, 2175-2188.
35 A. Tanaka, K. Nakashima, Y. Miura, *Tetrahedron* 2011, **67**, 2260-2268.
36 P. Verma, A. Perera, J. A. Morales, *J. Chem. Phys.* 2013, **139**, 174103.
37 X. Chen, Z. Rinkevicius, K. Ruud, H. Ågren, *J. Chem. Phys.* 2013, **138**, 054310.
38 A. D. Becke, *J. Chem. Phys.* 1993, **98**, 5648-5652.
39 C. T. Lee, W. T. Yang, R. G. Parr, *Phys. Rev. B* 1988, **37**, 785-789.
40 N. Godbout, D. R. Salahub, J. Andzelm, E. Wimmer, *Can. J. Chem.* 1992, **70 (2)**, 560-571.
41 N.Rega, M. Cossi, V. Barone, *J. Chem. Phys.* 1996, **105 (24)**, 11060-11067.
42 V. Barone, *J. Phys. Chem.* 1995, **99 (30)**, 11659-11666.
43 J. Barilone, F. Neese, M. van Gastel, *Appl. Magn. Reson.* 2015, **46**, 117-139.
44 W. J. Hehre, R. Ditchfield, J. A. Pople, *J. Chem. Phys.* 1972, **56**, 2257-2261.
45 R. Krishnan, J. S. Binkley, R. Seeger, J. A. Pople, *J. Chem. Phys.* 1980, **72**, 650-654.
46 C. Adamo, V. Barone, *J. Chem. Phys.* 1999, **110**, 6158-6170.
47 L. Hermosilla, G. Prampolini, P. Calle, J. M. García de la Vega, G. Brancato, V. Barone, *J. Chem. Theory Comput.* 2013, **9**, 3626-3636.
48 V. Barone, R. Improta, N. Rega, *Acc. Chem. Res.* 2008, **41 (5)**, 605-616.
49 P. Cimino, A. Pedone, E. Stendardo, V. Barone, *Phys. Chem. Chem. Phys.* 2010, **12**, 3741-3746.
50 E. Stendardo, A. Pedone, P. Cimino, M. C. Menziani, O. Crescenzi, V. Barone, *Phys. Chem. Chem. Phys.* 2010, **12**, 11697-11709.
51 M. Pavone, M. Biczysko, N. Rega, V.Barone, *J. Phys. Chem. B* 2010, **114**, 11509-11514.
52 C. Houriez, N. Ferré, D. P. Siri, Tordo, M. Masella, *J. Phys. Chem. B* 2010, **114 (36)**, 11793-11803.
53 C. Houriez, N. Ferré, D. Siri, P. Tordo, M. Masella, *Theor. Chem. Acc.* 2012, **131 (6)**, 1240-1244.
54 R. A. Kendall, T. H. Dunning Jr., R. J. Harrison, *J. Chem. Phys.* 1992, **96**, 6796-6806.
55 Gaussian 09, Revision A.02, M. J. Frisch, G. W. Trucks, H. B. Schlegel, G. E. Scuseria, M. A. Robb, J. R. Cheeseman, G. Scalmani, V. Barone, B. Mennucci, G. A. Petersson, H. Nakatsuji, M. Caricato, X. Li, H. P. Hratchian, A. F. Izmaylov, J. Bloino, G. Zheng, J. L. Sonnenberg, M. Hada, M. Ehara, K. Toyota, R. Fukuda, J. Hasegawa, M. Ishida, T. Nakajima, Y. Honda, O. Kitao, H. Nakai, T. Vreven, J. A. Montgomery, Jr., J. E. Peralta, F. Ogliaro, M. Bearpark, J. J. Heyd, E. Brothers, K. N. Kudin, V. N. Staroverov, R. Kobayashi, J. Normand, K. Raghavachari, A. Rendell, J. C. Burant, S. S. Iyengar, J. Tomasi, M. Cossi, N. Rega, J. M. Millam, M. Klene, J. E. Knox, J. B. Cross, V. Bakken, Adamo, J. Jaramillo, R. Gomperts, R. E. Stratmann, O. Yazyev, A. J. Austin, R. Cammi, C. Pomelli, J. W. Ochterski, R. L. Martin, K. Morokuma, V. G. Zakrzewski, G. A. Voth, P. Salvador, J. J. Dannenberg, S. Dapprich, A. D. Daniels, Ö. Farkas, J. B. Foresman, J. V. Ortiz, J. Cioslowski, and D. J. Fox, Gaussian, Inc., Wallingford CT, 2009.
56 R. López, J. Fernández-Rico, G. Ramírez, I. Ema, D. Zorrilla, *Comput. Phys. Comm.* 2015, **192**, 289-294.
57 J. Fernández-Rico, R. López, G. Ramírez, *J. Chem. Phys.* 1999, **110**, 4213-4220.
58 J. Fernández-Rico, R. López, I. Ema, G. Ramírez, *J. Chem. Phys.* 2002, **117**, 533-540.
59 J. Fernández-Rico, R. López, G. Ramírez, I. Ema, E. V. Ludeña, *J. Comput. Chem.* 2004, **25**, 1355-1363.
60 J. Fernández-Rico, R. López, I. Ema, G. Ramírez, *J. Chem. Theory Comput.* 2005, **1**, 1083-1095.
61 A. G. Davies, L. Julia, S. N. Yazdi, *J. Chem. Soc., Chem. Commun.* 1987, 929-930.
62 A. G. Davies, L. Julia, S. N. Yazdi, *J. Chem. Soc., Perkin Trans. 2* 1989, 239-244.
63 B. L. Barton, G. K. Fraenkel, *J. Chem. Phys.* 1964, **41**, 1455-1468.
64 M.-K. Ahn, Charles S. Johnson Jr. *J. Chem. Phys.* 1969, **50**, 632-640.
65 W. Kaim, *Heterocycles,* 1985, **23**, 1363-1366.
66 P. D. Sullivan, W. W. Paudler, *Can. J. Chem.* 1973, **51**, 4095-4097.
67 R. F. Nelson, D. W. Leedy, E. T. Seo, R. N. Adams, *Fresenius J. Anal. Chem.* 1966, **224**, 184-196.
68 P. D. Sullivan, J. Y. Fong, M. L. Williams, V. D. Parker, *J. Phys. Chem.* 1978, **82**, 1181-1185.
69 P. D. Sullivan, M. L. Williams, *J. Am. Chem. Soc.* 1976, **98**, 1711-1716.
70 C. S. Johnson Jr., H. S. Gutowsky, *J. Chem. Phys.* 1963, **39**, 58-62.
71 J. Bruhin, F. Gerson, *Helv. Chim. Acta* 1975, **58**, 2422-2431.
72 F. Gerson, J. Jachimowicz, D. Leaver, *J. Am. Chem. Soc.* 1973, **95**, 6702-6708.
73 F. Gerson, A. Lamprecht, *Helv. Chim. Acta* 1994, **77**, 86-91.
74 P. D. Sullivan, J. R. Bolton, *J. Magn. Reson.* 1969, **1**, 356-361.
75 B. C. Gilbert, R. H. Schlossel, W. M. Gulick, *J. Am. Chem. Soc.* 1970, **92**, 2974-2982.
76 F. A. Neugebauer, S. Bamberger, W. R. Groh, *Chem. Ber.* 1975, **108**, 2406-2415.
77 B. M. Latta, R. W. Taft, *J. Am. Chem. Soc.* 1967, **89**, 5177-5178.

78 M. T. Melchior, A. H. Maki, *J. Chem. Phys.* 1961, **34**, 471-476.
79 M. R. Das, G. K. Fraenkel, *J. Chem. Phys.* 1965, **42**, 792-794.
80 K. H. Hausser, *Mol. Phys.* 1964, **7 (2)**, 195-195.
81 K. Elbl-Weiser, F. A. Neugebauer, H. A. Staab, *Tetrahedron Lett.* 1989, **30**, 6161-6164.
82 G. Grampp, A.-M. Kelterer, S. Landgraf, M. Sacher, D. Niethammer, J. P. Telo, R. M. B. Dias, A. J. S. C. Vieira, *Monatsh. Chem.* 2005, **136**, 519-536.
83 J. S. Miller, D. A. Dixon, J. C. Calabrese, C. Vazquez, P. J. Krusic, M. D. Ward, E. Wasserman, R. L. Harlow, *J. Am. Chem. Soc.* 1990, **112**, 381-398.
84 P. Smejtek, J. Honzl, V. Metalová, *Collect. Czech. Chem. Commun.* 1965, **30**, 3875-3889.
85 S. Bamberger, D. Hellwinkel, F. A. Neugebauer, *Chem. Ber.* 1975, **108**, 2416-2421.
86 H. Zeldes, R. Livingston, *J. Phys. Chem.* 1972, **76 (23)**, 3348-3355.
87 F. A. Neugebauer, H. Weger, *J. Phys. Chem.* 1978, **82**, 1152-1157.
88 F. A. Neugebauer, M. Bock, S. Kuhnhäuser, H. Kurreck, *Chem. Ber.* 1986, **119**, 980-990.
89 F. Gerson, G. Gescheidt, J. Knoebel, W. B. Martin, L. Neumann, E. Vogel, *J. Am. Chem. Soc.* 1992, **114**, 7107-7115.
90 F. Gerson, J. Knoebel, U. Buser, E. Vogel, M. Zehnder, *J. Am. Chem. Soc.* 1986, **108**, 3781-3783.
91 F. Gerson, G. Gescheidt, U. Buser, E. Vogel, J. Lex, M. Zehnder, A. Riesen, *Angew. Chem. Int. Ed. Engl.* 1989, **28**, 902-904.
92 T. Bally, C. Carra, S. Matzinger, L. Truttmann, F. Gerson, R. Schmidlin, M. S. Platz, A. Admasu, *J. Am. Chem. Soc.* 1999, **121**, 7011-7019.
93 F. Gerson, W. Huber, Conjugated Radicals with Heteroatoms. In *Electron Spin Resonance Spectroscopy of Organic Radicals* Wiley-VCH: Weinheim, Germany, 2003 pp 37-48.
94 J. M. Zwier, A. M. Brouwer, T. Keszthelyi, G. Balakrishnan, J. F. Offersgaard, R. Wilbrandt, F. Barbosa, U. Buser, J. Amaudrut, G. Gescheidt, S. F. Nelsen, C. D. Little, *J. Am. Chem. Soc.* 2002, **124 (1)**, 159-167.